



## Wavefront phase calculation of optical vector beams using phase shifting interferometry

P García-Martínez<sup>1</sup>, I Moreno<sup>2,3</sup> and M M Sánchez-López<sup>2,4</sup>

<sup>1</sup>Department of Optics and Optometry and Vision Science, Faculty of Physics, University of Valencia, 46100 Burjassot (Valencia), Spain

<sup>2</sup>Bioengineering Institute, Miguel Hernández University, 03202 Elche, Spain

<sup>3</sup>Department of Materials Science, Optics and Electronics Technology, Miguel Hernández University, 03202 Elche, Spain

<sup>4</sup>Department of Applied Physics, Miguel Hernández University, 03202 Elche, Spain

Dedicated to Prof Maria J Yzuel

Recently, we proposed and built an optical system to generate arbitrary vector beams (VB) using two liquid-crystal on silicon (LCoS) spatial light modulators (SLM). Since the LCoS-SLMs devices used in the system are flicker-free, we showed the generation of VBs on-axis in a common path architecture being very efficient in terms of light energy. Here, we further demonstrate that the same system is also useful to perform common-path phase-shifting interferometry, thus being a useful tool to evaluate the phase distribution of the generated optical VB. We show different VBs obtained by superposition of two Laguerre-Gaussian (LG) beams with different orthogonal polarizations. The phase measurement is obtained by phase shifting interferometry (PSI), obtained by adding different values of a uniform phase distribution in one of the SLMs, and registering the corresponding interferograms. The continuous phase modulation provided by the LCoS-SLMs is demonstrated here to be useful to apply the synchronous detection interferometric technique for the verification of the phase distribution of different VBs. © Anita Publications. All rights reserved.

**Keywords:** Vector modes, Laguerre-Gaussian Beams, Vector beams, Interferometry, LCoS, Phase Shifting.

### 1 Introduction

Vector beams (VBs), as light beams with defined spatially-variant intensity, phase and polarization features, are important for many applications including tight focusing [1], optical tweezing [2], materials processing [3], or super-resolution microscopy [4]. VBs can also be defined as pure laser modes with an additional spatial polarization modulation [5]. There have been several methods to generate such beams, based on the superposition of scalar modes having orthogonal polarization [6]. Initial techniques included the manipulation of a laser resonator in order to directly emit a desired vector beam [7], or the use of interferometric arrangements [8]. More recently, they have been generated with spatially variant uniaxial flat elements, which can be fabricated with subwavelength gratings [9], or with liquid-crystal materials [10]. These elements, often referred to as q-plates, are in general designed to generate low-order VBs [11,12]. However, higher-order Laguerre-Gaussian q-plates have also been developed [13].

In addition, optical beams with helical wave-fronts and associated orbital angular momentum (OAM) have become a focus of intense research in recent years owing to its high-capacity information

---

Corresponding author

e mail: [pascuala.garcia@uv.es](mailto:pascuala.garcia@uv.es) (P García-Martínez)

bearing characteristics with noteworthy applications in various domains of imaging and communication [14]. The recognition of OAM of helical phase beams provides new insights into the theoretical and applied realms of optical vortex beams [14]. The vortex encoded light beams possess an azimuthal phase of  $e^{i\ell\theta}$ , where  $\theta$  is the angular coordinate and  $\ell$  is referred to topological charge that owns a positive or negative sign, and carries an OAM equivalent to  $\ell\hbar$  per photon [5]. The topological charge equals the number of ring dislocations in its far field amplitude. Paradigmatic examples of light beams with such spiral phase patterns are Laguerre-Gauss beams.

Besides, the advancements in the generation of vector beams, vortex beams and other higher order modes motivated their application for optical communications [15-17]. In this context, the recovery and determination of topological charge of optical vortex beams have been receiving much attention during last decade [18,19]. More recently, Prabhakar *et al* [20] proposed a method for determining the topological charge of a vortex beam through measuring the Fourier transform (FT) of its intensity, and it was shown that the number of the dark rings in the FT of the intensity is equal to the topological charge of the vortex beams. In fact, conventional approaches for measuring topological charges are mostly based on diffraction fringe counting or intensity analysis [21,22]. However, given the defects of these optical elements and the noisy illumination background, these methods can roughly distinguish vortex beams with significant differences in their topological charges instead of offering a precise measurement of these topological charges. Other techniques exploit the correlation between the input beam and reference beams encoded onto a diffraction grating or holograms, typically encoded onto phase-only SLMs [23,24].

Topological charge can also be estimated by recovering the phase distribution of the beam. This is advantageous since any defect in the generation of phase distribution can be directly visualized on the phase pattern. Examples include the use of a phase-only SLM as a phase-shifting element within a Mach-Zehnder interferometer [25] or with ghost diffraction holography [26]. In this paper, we present a different method based on phase shifting technique to directly obtain the phase distribution of superposition of LG beams and so the topological charge can be obtained. We use a previously reported optical system [27] to efficiently generate vector beams by means of two liquid-crystal on silicon (LCOS) SLMs, each one encoding a phase pattern onto an orthogonal polarization component. By adding a polarizer at the output, the interference of the two polarization components is obtained. Here we take profit of the possibility of adding a constant phase value to any of the two SLMs to produce an arbitrary phase shift. Because this phase shift can be made continuous, the synchronous detection method [28,29] can be applied by recording an arbitrary number  $N$  of intensity interference patterns useful to obtain the phase recovery of the output beam through PSI.

The paper is organized as follows: after this introduction, Section 2 describes the interferometric optical system to generate the LG modes. Vector beams and OAM are treated in Section 3. In Section 4, we explain the phase-shifting techniques to recover the phase distribution of the generated beams. Experimental results are shown in Section 5. Finally, conclusions are given in section 6.

## 2 Interferometric experimental optical setup

Figure 1 shows the scheme of the optical system [27]. We use an input He-Ne laser ( $\lambda = 633$  nm) that is spatially filtered and collimated. Two LCoS-SLMs are arranged in a Z configuration. The angle between the incident ray and the reflected ray on each modulator is about  $11^\circ$ . LCoS1 and LCoS2 devices are on conjugated planes by means of a 4f-system obtained by two lenses of the same focal length, thus obtaining a minus one magnification. Both devices are parallel-aligned LCoS displays from Hamamatsu (model X10468-01). We measured a reflectivity of more than  $R = 78\%$  for both devices. We also measured more than  $2\pi$  radians of phase modulation for the operating wavelength [30]. And they have  $800 \times 600$  pixels, with  $20 \mu\text{m}$  pixel pitch, an effective area of  $15.8 \times 12 \text{ mm}^2$  and 98% fill factor, thus providing more than 96% efficiency to

the main reflected beam (zero order). Therefore, the total device efficiency at the zero order is about  $\eta \sim 75\%$ . As mentioned earlier, an important characteristic of these devices is that they are free of flicker. Therefore, the reflected beam does not present zero order (DC) component and the displayed holograms can be designed to generate hologram reconstruction on-axis, and therefore make full use of this 75% zero-order efficiency [31].

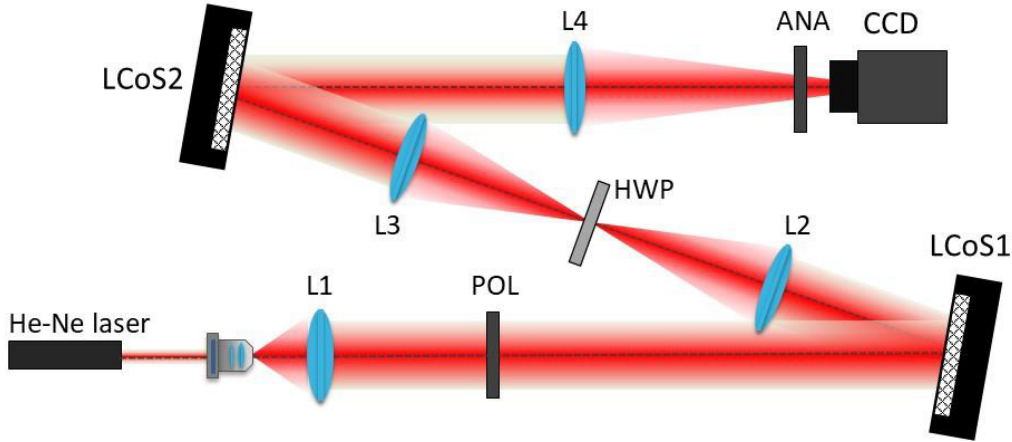


**Fig 1.** Scheme of the optical setup. LCoS1 and LCoS2 are liquid-crystal on silicon SLMs, with the liquid-crystal director oriented horizontally. A 4f-system (lenses L2 and L3) gives an image of LCoS1 into LCoS2. POL: input linear polarizer. ANA: output polarization analyzer. HWP: half-wave plate. CCD: charge couple device detector.

The input polarizer (POL) is oriented at  $45^\circ$  to ensure equal magnitude on both horizontal and vertical polarization components. Parallel-aligned LCoS displays only modulation of the linear polarization component which is parallel to the LC director. In our laboratory devices, this corresponds to the horizontal direction. Therefore, a phase pattern addressed to LCoS1 modulates the horizontal component of the input beam, while the vertical polarization component remains unaffected. A half-wave plate (HWP) oriented at  $45^\circ$  is added after LCoS1 in order to transform the horizontal linear polarization component into the vertical component of the input beam (and vice-versa). In this way, LCoS2-SLM modulates the polarization component that was not modulated by LCoS1-SLM, while leaving unaffected the polarization component that was already modulated by the first SLM. Thus, the output beam has two orthogonal horizontal and vertical polarization components that are independently modulated through the phase-only mask implemented by the two LCoS-SLMs.

Since, the output beam emerging from the system is a phase-only distribution in its vertical and horizontal components, therefore, the output Jones vector can be written as:

$$\vec{J}(x, y) = \begin{pmatrix} J_x(x, y) \\ J_y(x, y) \end{pmatrix} = \begin{pmatrix} e^{i\psi_1(x, y)} \\ e^{i\psi_2(x, y)} \end{pmatrix}, \quad (1)$$

where  $J_x(x, y)$  and  $J_y(x, y)$  denote the spatial patterns encoded onto the vertical and horizontal linear polarization components, respectively, and  $e^{i\psi_k(x, y)}$ ,  $k = 1, 2$  denotes the phase-only mask displayed onto LCoS1 and LCoS2 SLMs, respectively. A converging lens is introduced to focus the beam in a CCD camera (see lens L4 in Fig 1). In our optical system the converging lens has been simulated by encoding it as a phase-only hologram in the SLM. Finally, a polarizer analyzer (ANA) verifies the polarization output.

Since LCoS-SLM devices work in phase-only modulation regime, a method to encode complex values onto phase-only displays is required. Here, we used the codification method described in [32], which is based on a random spatial multiplexing of two phase-only functions: the phase information of the desired pattern and a diverging optical diffractive element to redirect undesired light out of the optical axis. This

codification method presents interesting features: (1) it does not require any iterative algorithms, thus it is not computationally costly; (2) the desired complex optical field is reconstructed on-axis; and (3) no phase carriers are required. Next, we briefly review this method.

Let  $F(x, y) = M(x, y) e^{i\varphi(x, y)}$  be the complex function to be encoded, where  $M(x, y)$  and  $\varphi(x, y)$  represent its magnitude and phase. A new multiplexed phase-only function  $e^{i\psi(x, y)}$  is designed as:

$$e^{i\psi(x, y)} = R(x, y) e^{i\varphi(x, y)} + \bar{R}(x, y) e^{i\zeta(x, y)} \quad (2)$$

where  $R(x, y)$  is a binary-amplitude (0-1) pattern,  $\bar{R}(x, y) = 1 - R(x, y)$  is its complementary pattern, and  $e^{i\zeta(x, y)}$  is the phase function of a diverging element, in our case a high-frequency negative diffractive axicon,  $\zeta(x, y) = -2\pi r/p$ , where  $r = \sqrt{(x^2 + y^2)}$  denotes the radial coordinate, and  $p$  denotes the axicon's period.

The negative diffractive axicon acts as a circular blazed diffraction grating that diverges the light away from the optical axis. This light can be very easily filtered by a circular aperture. This way, the magnitude information  $M(x, y)$  is encoded onto the new multiplexed phase-only function  $\psi(x, y)$  via the function  $R(x, y)$  which is defined as

$$R(x, y) = \begin{cases} 1 & \text{if } M(x, y) > rnd(x, y) \\ 0 & \text{if } M(x, y) \leq rnd(x, y) \end{cases} \quad (3)$$

where,  $rnd(x, y)$  is a distribution of random numbers in the interval  $[0,1]$ .

This phase-only encoding technique of the complex function  $M(x, y) e^{i\varphi(x, y)}$  can be easily understood as follows. If the required amplitude  $M(x, y)$ , is close to 1, it is better represented by the phase-only function  $e^{i\varphi(x, y)}$  and  $R(x, y) = 1$  is the good choice. On the contrary, for pixels where  $M(x, y)$  is close to 0, light should be removed. The diverging axicon performs this operation directing light out of the optical axis. Therefore,  $R(x, y) = 0$ , is the right choice for these pixels. For intermediate values of  $M(x, y)$ , Eqs(2-3) provide an adequate random choice between the two phase-only functions.

### 3 Generation of vector beams as Laguerre-Gauss modes superposition

In this work, we encode Laguerre Gaussian modes on the  $J_x(x, y)$  and  $J_y(x, y)$  patterns. LG modes are exact solutions of the scalar paraxial wave equations in cylindrical coordinates. We consider an output beam at the waist plane  $z = 0$ , the complex amplitude can thus be written as:

$$LG_p^\ell(r, \theta, \omega_0) = \frac{1}{\omega_0} \frac{p! 2^{|\ell|+1}}{\sqrt{\pi} (|\ell| + p)!} \left(\frac{r}{\omega_0}\right)^{|\ell|} L_p^{|\ell|} \left(\frac{2}{\omega_0^2} r^2\right) e^{-(r/\omega_0)^2} e^{i\ell\theta} = A_{p\ell}(r) e^{i\ell\theta} \quad (4)$$

where  $L_p^{|\ell|}$  are the  $p$ -th order Laguerre polynomials, and  $r$  and  $\theta$  are polar coordinates. The term  $A_{p\ell}(r)$  in this equation accounts for the radial part of the function and does not depend on the sign of  $\ell$ , only on its magnitude. The mode order is  $N = 2p + |\ell|$  for a LG mode [33].

Although VBs are natural solutions to the vectorial Helmholtz equation they are very often generated as coaxial superpositions of orthogonal scalar fields with orthogonal polarizations [6]. The system in Fig 1 directly allows the superposition of different LG modes encoded on the vertical and horizontal polarization states. For instance, we generate higher-order vector beams by combining LG modes with orthogonal polarization states and higher values. We used again the linear polarization basis  $(x, y)$  that comes from the system in Fig 1. Therefore, the output vector beam can be written as the following Jones vector:

$$\vec{J}(r, \theta) = \begin{pmatrix} J_x(r, \theta) \\ J_y(r, \theta) \end{pmatrix} = \begin{pmatrix} LG_{p_1}^{\ell_1}(r, \theta) \\ LG_{p_2}^{\ell_2}(r, \theta) \end{pmatrix} = \begin{pmatrix} A_{(p_1, \ell_1)}(r) e^{i\ell_1\theta} \\ A_{(p_2, \ell_2)}(r) e^{i\ell_2\theta} \end{pmatrix} \quad (5)$$

The corresponding intensities of the superposed beam behind a linear polarizer at different rotation angles is then calculated by projecting the electric field vector on the corresponding linear polarization states. When we use a linear analyzer oriented horizontal and vertical axis, we recover the distribution given by

$LG_{p_1}^{\ell_1}(r, \theta)$  and  $LG_{p_2}^{\ell_2}(r, \theta)$ , respectively. If the analyzer is oriented at  $\pm 45^\circ$ , the following superposition is obtained.

$$\vec{J}_A = \frac{1}{2} \begin{pmatrix} 1 & \pm 1 \\ \pm 1 & 1 \end{pmatrix} \vec{J}(r, \theta) = \frac{1}{\sqrt{2}} (LG_{p_1}^{\ell_1} \pm LG_{p_2}^{\ell_2}) \vec{P}_{\pm 45} \quad (6)$$

where,  $\vec{P}_{\pm 45}$  is the linear polarization normalized state at  $\pm 45^\circ$ .

We can calculate the corresponding intensity by squaring the absolute values of the electric field, as in an interferometric optical system, which will be developed in next section.

#### 4 Determination of VB wavefront phase using phase-shifting interferometry

PSI is a well-established technique for areal surface characterization that relies on digitalization of interference data acquired with a controlled phase shift, most often introduced by controlled mechanical oscillation [28,29]. The last years have seen many significant developments in PSI [34,35]. The PSI is based on the recording of different interferograms by introducing artificially known steps of phase differences in the interference pattern as:

$$I_j(x, y) = I_0(x, y) \{1 + V(x, y) \cos[\alpha(x, y) + \delta_j]\} \quad (7)$$

where  $I_0(x, y)$  is the mean intensity,  $V(x, y)$  is the visibility,  $\alpha(x, y)$  is the phase difference between the interfering waves and  $\delta_j$  is the phase shift which is produced by adding a phase term in one of the interferogram path. A minimum of three intensity patterns are required to calculate the phase distribution [30]. In our case we used a technique known as synchronous detection, that consist of recording  $N$  stepped phase interferograms and then calculating the phase distribution as:

$$\alpha(x, y) = \tan^{-1} \left[ \frac{\sum_{j=1}^N I_j(x, y) \sin \delta_j}{\sum_{j=1}^N I_j(x, y) \cos \delta_j} \right] \quad (8)$$

where,  $\delta_j = 2\pi j/N$  is the phase shift for the  $j$ th interferogram,  $I_j(x, y)$  is the corresponding intensity of the interference pattern, and  $N$  is the total number of phase steps.

One of the common methods for introducing the phase shifts in an interferometer is moving a mirror mounted on a piezoelectric transducer (PZT). The role of the PZT is to shorten or elongate the reference beam path by a fraction of a wavelength [28,29]. Here, instead, we will make use of the phase-modulation property of the LCoS-SLM to add this phase bias, so the same system that generates the VBs is employed also for the phase-shifting measurement. Since, we illuminate the system with linearly polarized light oriented at  $45^\circ$ , we have equal intensity in vertical and horizontal polarization components, therefore achieving the maximum visibility in the interference. Because of that the function  $V(x, y)$  in Eq (7) is equal to one.

We are interested in the calculation of the phase of superposition of  $LG$  modes  $LG_{p_1}^{\ell_1}(r, \theta)$  and  $LG_{p_2}^{\ell_2}(r, \theta)$  obtained after they pass through the polarizer analyser oriented at  $45^\circ$ , i.e. the phase of the amplitude term of the Jones vector in Eq (6). The phase-only SLMs in the system also enable adding an extra constant relative phase-shift between the vertical and horizontal polarization components, i.e., this is equivalent to adding a linear retarder with retardance  $\delta$  and neutral axes oriented along vertical/horizontal directions. For instance, if we apply the phase shifting technique adding steps of phase in the second SLM, the output Jones vector after the addition of phase-shift  $\delta_j$  is given by

$$\vec{J}_j(x, y) = \vec{J}(r, \theta, \delta_j) = \begin{pmatrix} J_x(r, \theta) \\ J_y(r, \theta) e^{i\delta_j} \end{pmatrix} = \begin{pmatrix} A_{(p_1, \ell_1)}(r) e^{i\ell_1 \theta} \\ A_{(p_2, \ell_2)}(r) e^{i\ell_2 \theta} e^{i\delta_j} \end{pmatrix} \quad (9)$$

According to Eq (6), the intensity of the superposition when the analyzer is oriented at  $+45^\circ$  is given by

$$I_j(x, y) = \vec{J}_j(x, y) \vec{J}_j^\dagger(x, y) = |A_{(p_1, \ell_1)}|^2 + |A_{(p_2, \ell_2)}|^2 + 2A_{(p_1, \ell_1)}A_{(p_2, \ell_2)} \cos[\alpha(x, y) + \delta_j], \quad (10)$$

where now  $\alpha = (\ell_1 - \ell_2)\theta$ . Then, the phase distribution  $\alpha(x, y)$  of the superposition of the *LG* modes is directly calculated from Eq (8).

## 5 Experimental results

In this final subsection, we generate higher-order vector beams by combining *LG* modes encoded in orthogonal polarization states and higher  $\ell$  values. We used again the linear polarization basis  $(x, y)$  that naturally comes from the system in Fig 1.

### 5.1. Calibration of the phase modulation

We first calibrated the phase modulation to properly apply the PSI algorithm. For that purpose, the input polarizer in the system was oriented at  $45^\circ$  while the output polarizer was oriented crossed, oriented at  $-45^\circ$ . This configuration has been used extensively to measure the retardance of linear retarders [36] which can be derived directly from intensity measurements. If both SLMs display the same amplitude and a uniform phase pattern, in Eq (10) we can consider the amplitude terms as constant,  $\alpha(x, y) = 0$ ; and therefore, the intensity is given directly proportional to  $(1 + \cos(\delta_i))$ . The images in Fig 2 were captured in the camera detector when images with uniform gray level were displayed in both LCoS1 and LCoS2 SLMs, but the gray value was varied in the first SLM. The images show a complete oscillation in the intensity, thus denoting the phase change of  $2\pi$  radians.

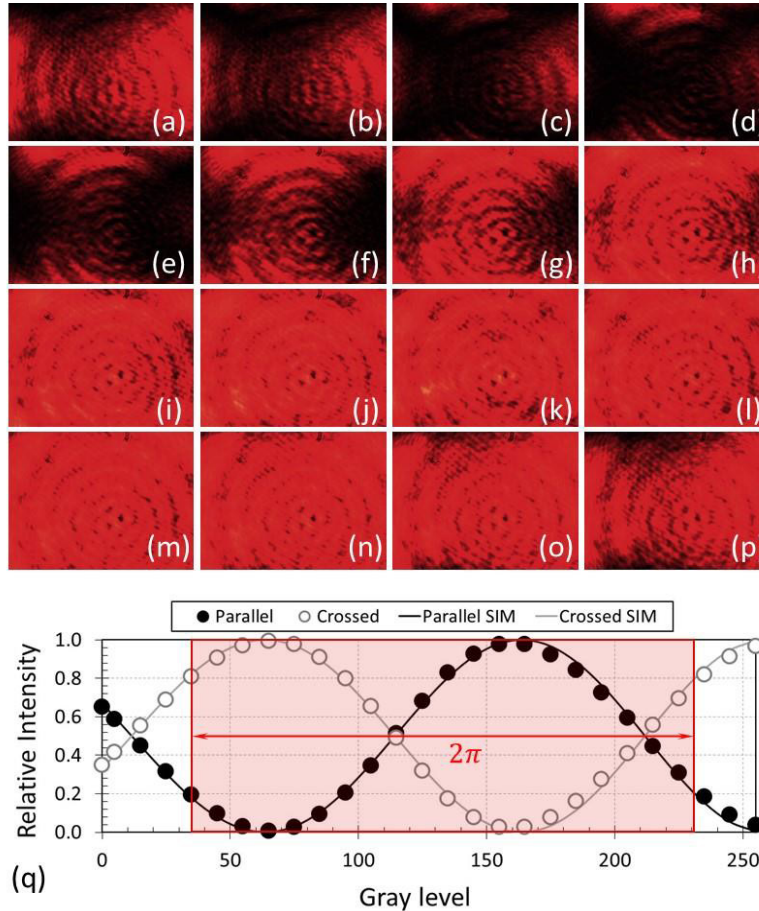


Fig 2. (a)-(p) Images captured in the CCD camera when the LCoS-SLMS are addressed with uniform images. Input and output polarizers are oriented at  $+45^\circ$  and  $-45^\circ$ , respectively. The gray level is varied in each image in steps of  $\pi/8$  radians.

Figure 2(q) shows the values measured for the intensity in this configuration, both with crossed and parallel polarizers, showing how the intensity follows the sinusoidal curve, with the  $2\pi$  phase modulation obtained for a gray level variation of about 200 levels. The images in Figs 2(a)-2(p) correspond to phase shifts added in LCoS1-SLM in steps of  $\delta_j = \pi/8$  radians obtained by changing the gray levels in steps of 12. We will use this phase shift as the bias for the PSI procedure.

### 5.2. Superposition of two LG modes with zero radial index and opposite azimuthal indexes

Once the system is calibrated, we can use it to display phase masks generating the desired modes. Figure 3(a) and 3(b) shows the phase functions (encoded in gray levels) that are addressed to LCoS-SLM1 and LCoS-SLM2 in Fig 1, respectively. These phase functions encode the amplitude and phase of the LG modes  $LG_{03}$  and  $LG_{0-3}$ , respectively, but also codify an additional quadratic phase that reproduces the effect of the lens L4 in the system in Fig 1. Note how the spiral phase characteristic of the LG modes are clearly encoded in the phase pattern, showing opposite sense. Figure 3(c) shows a computer simulation of the intensity distribution and state of polarization of the generated VB by this superposition. In this figure, the opposite helicity of the polarization ellipses is indicated in red/blue colours, while green denotes linear states. This result shows how the ellipticity of this VB is changing azimuthally. Figure 3(d) shows the expected intensity distribution when the beam is filtered with a linear polarizer oriented at  $45^\circ$ , and the experimentally captured intensity pattern in the plane of focusing is shown in Fig 3(e). This focalization is in the form of a “petal” beam [37]. The annular focusing characteristic of the  $LG_{0\ell}$  mode has the same radius since  $\ell = \ell_1 = -\ell_2$ . Since both modes share the same amplitude, Eq (10) now turns to be

$$I_j(x, y) = 2|A_0\ell|^2(1 + \cos [2\ell\theta + \delta_j]) = 4|A_0\ell|^2 \cos^2 \left( \ell\theta + \frac{\delta_j}{2} \right), \quad (11)$$

where we used that  $\alpha(\theta) = (\ell_1 - \ell_2)\theta = 2\ell\theta$ . This function is represented in Fig 3 (f). Therefore, if we consider  $\delta_0 = 0$ , the maxima of the cosine function is obtained when  $\ell\theta = m\pi$  i.e. at angles  $\theta = m\pi/\ell$ . Consequently, since we selected in this case  $\ell=3$ , the maxima are located at angles  $\theta_0 = 0^\circ$ ,  $\theta_1 = 60^\circ$ ,  $\theta_2 = 120^\circ$ ,  $\theta_3 = 180^\circ$ ,  $\theta_4 = 240^\circ$ , and  $\theta_5 = 300^\circ$ , with points of null intensity at angles in between, thus providing the six bright lobes pattern observed in the doughnut focalization shown in Fig 3(d-3e).

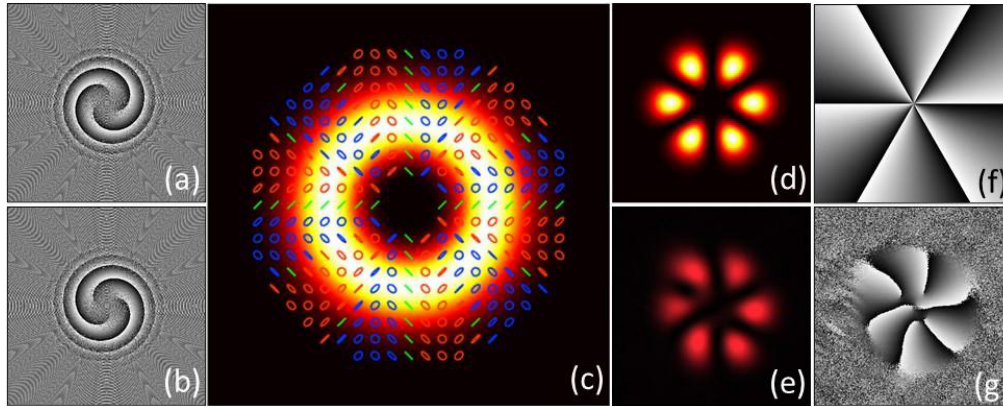


Fig 3. (a) and (b) Central part of the phase-only holograms displayed on LCoS1 and LCoS2 SLMs to generate  $LG_{03}$  and  $LG_{0-3}$  modes (c) Simulation of the intensity and polarization of the generated vector beam. (d-e) Intensity distribution after passing through a polarizer oriented at  $45^\circ$ , simulation and experiment. (f) Phase difference  $\alpha(x, y)$ . (g) Result obtained by PSI synchronous algorithm.

To experimentally measure the phase function  $\alpha(x, y)$  in this beam, we apply the synchronous detection algorithm of phase-shifting interferometry (PSI) [28]. In our system, we can apply this technique

via a constant phase-bias that can be added to the phase masks in any of the two LCoS-SLMs in the system. Figure 4 shows the experimental results obtained again from the superposition of the modes  $LG_{03}$  and  $LG_{0-3}$ , but now additional phase jumps of phase  $\delta_j = j\pi/8$ , where  $j = 0, 1, 2, \dots, 15$ . A new hologram like in Fig 2 (a) is calculated for each value of  $\delta_j$  and displayed on one of the SLM. The corresponding intensity patterns are shown in Fig 4. In all cases, we obtain the six-lobe annular pattern, but it is progressively rotated. As mentioned above, the beam is characterized by a phase  $\alpha(x, y) = 6\theta$ , thus with an azimuthal phase variation of  $2\pi$  radians every  $60^\circ$  in the transversal plane. Therefore, an additional phase bias of  $\pi/8$  radians in the phase modulation induce a rotation of the sidelobe pattern of an angle  $60^\circ \times \left(\frac{\pi/8}{2\pi}\right) = 3.75^\circ$ . The experimental results in Fig 4 corroborate this, where the rotation in steps of  $3.75^\circ$  is observed for every addition of  $\pi/8$  in the hologram displayed on the SLM.

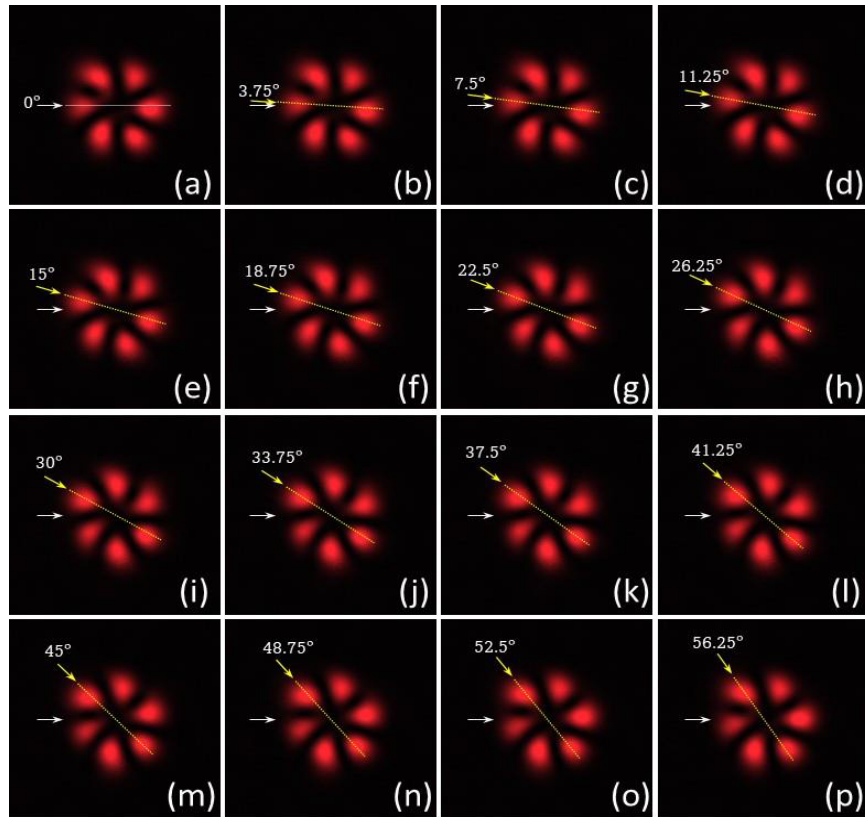


Fig 4. Experimental interferograms with superposition of  $LG_{03}$  and  $LG_{0-3}$  using phase steps of  $\pi/8$ .

These images in Fig 4 are then used to calculate the phase difference distribution  $\alpha(x, y)$  of the superposition with the PSI synchronous detection algorithm presented in Sec 3 and the result shown in Fig 3 (g). We can observe that the experimental superposition shows the expected spiral phase pattern with  $\ell = 3 - (-3) = 6$  jumps from 0 to  $2\pi$ . Thus, these results verify the correct generation of the vector beam, not only in terms of the intensity pattern (Fig 3(e)), but also in terms of its phase distribution (Fig 3(g)).

### 5.3. Comparison of vector and scalar vortex beams

When we encode  $LG$  modes with opposite topological charge (opposite azimuthal order) in orthogonal polarization states, we generate pure vector beams, but when we encode the same modes in both polarizations, we generate a scalar beam. To prove this, in this subsection we compare a situation where

modes  $LG_{09}$  and  $LG_{0,-9}$  are encoded in LCoS1 and LCoS2 SLMs with that where both SLMs encode the same mode  $LG_{0,-9}$ . This situation is the same as that in Sec 5.2 but with different opposite order values.

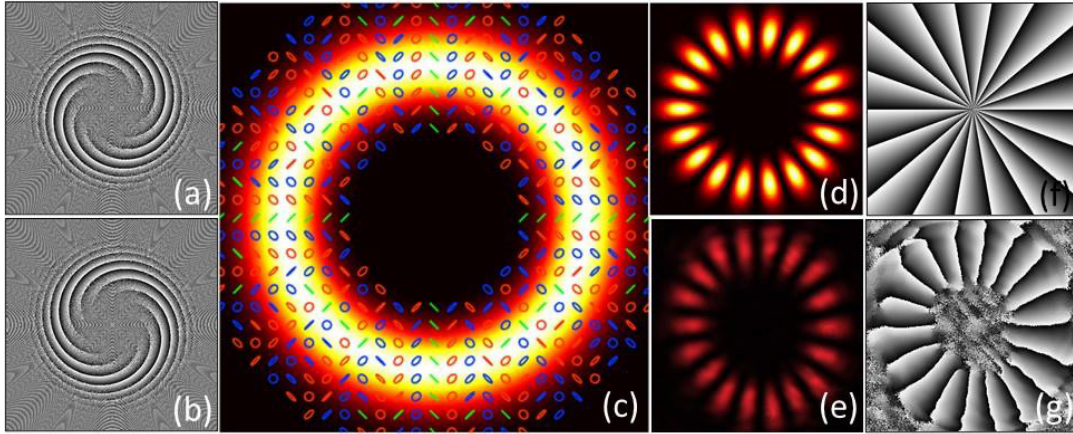


**Fig 5.** (a) and (b) Central part of the phase-only holograms displayed on LCoS1 and LCoS2 SLMs to generate  $LG_{09}$  and  $LG_{0,-9}$  modes. (c) Simulation of the intensity and polarization of the generated vector beam. (d-e) Intensity distribution after passing through a polarizer oriented at  $45^\circ$ , simulation and experiment. (f) Phase difference  $\alpha(x, y)$ . (g) Result obtained by PSI synchronous algorithm.

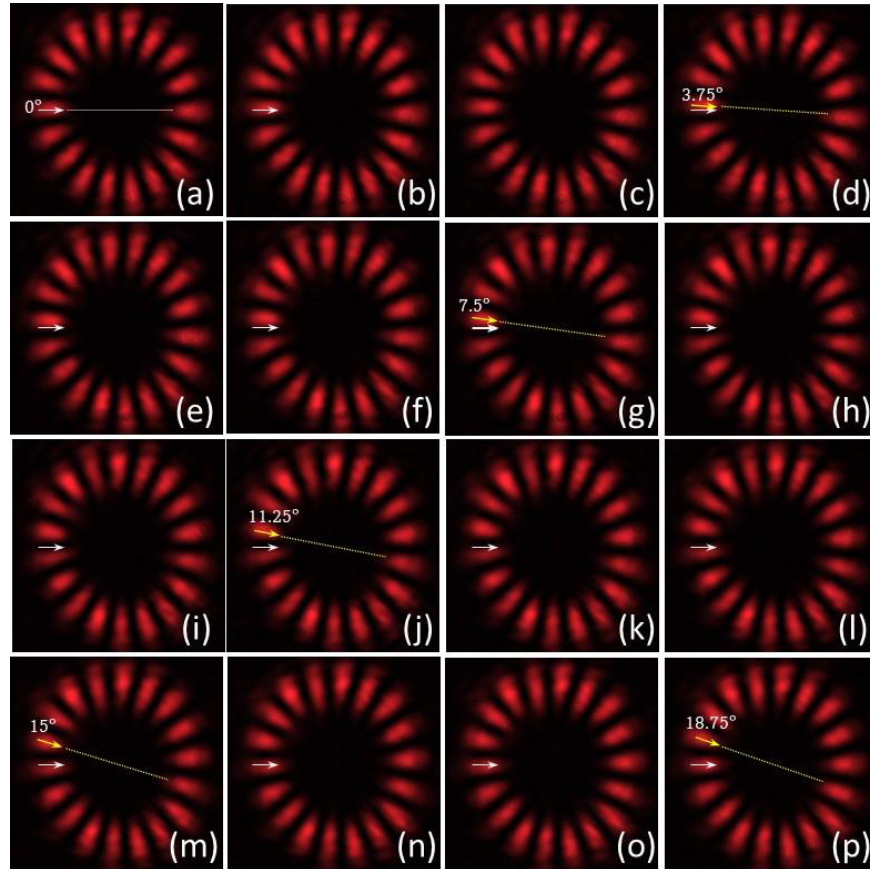


**Fig 6.** Experimental interferograms with superposition of  $LG_{09}$  and  $LG_{0,-9}$  using phase steps of  $\pi/8$ .

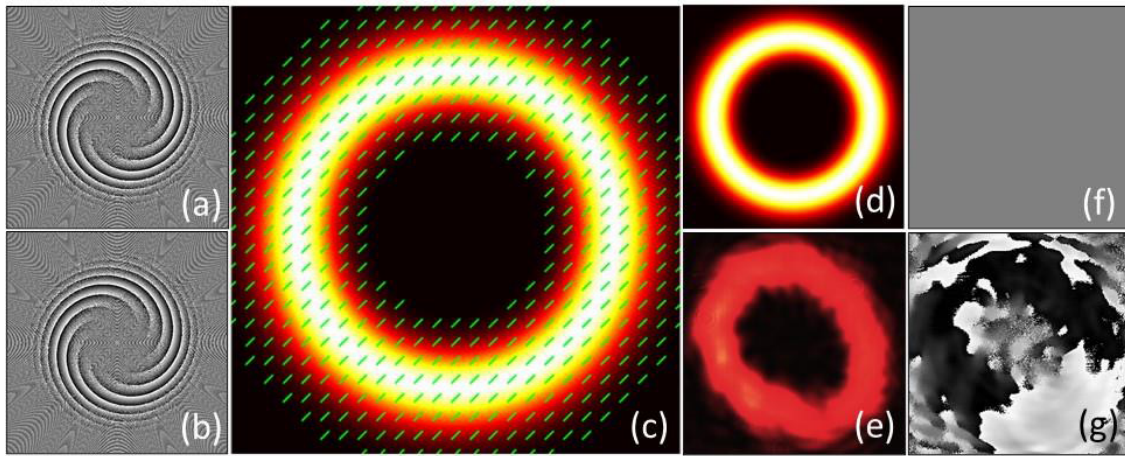


**Fig 7.** (a) and (b) Central part of the phase-only holograms displayed on LCoS1 and LCoS2 SLMs to generate  $LG_{00}$  mode in both SLMs. (c) Simulation of the intensity and polarization of the generated vector beam. (d-e) Intensity distribution after passing through a polarizer oriented at  $45^\circ$ , simulation and experiment. (f) Phase difference  $\alpha(x, y)$ . (g) Result obtained by PSI synchronous algorithm.

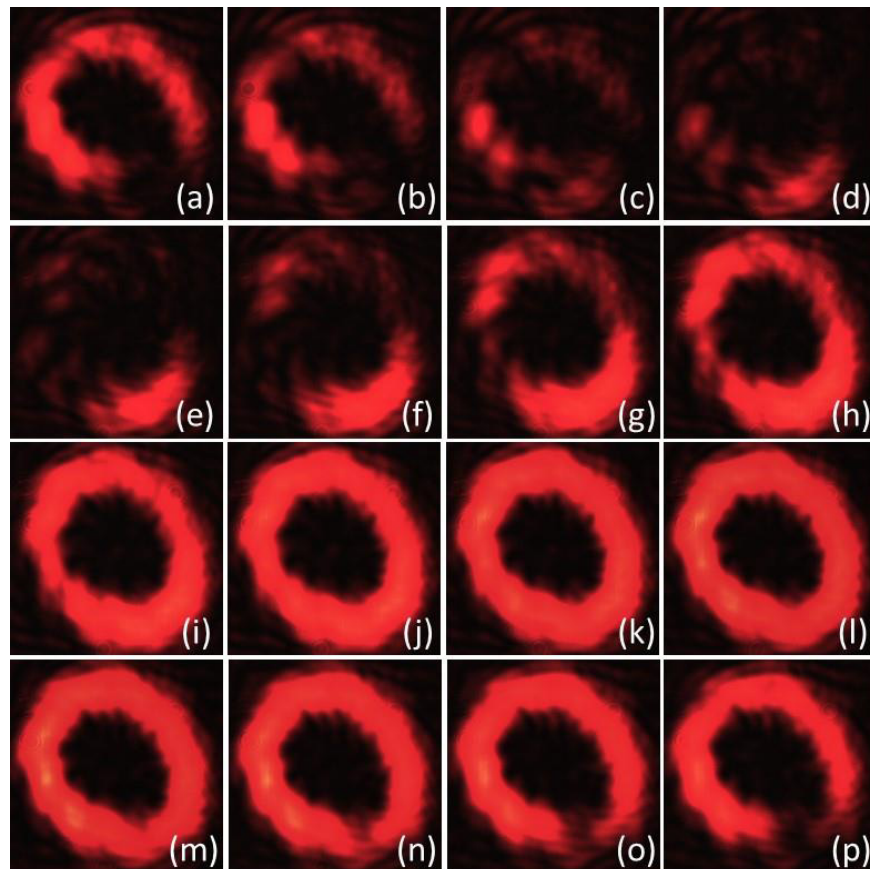


**Fig 8.** Experimental interferograms with superposition of two  $LG_{00}$  modes using phase steps of  $\pi/8$ .

Figures 5(a) and 5(b) show the holograms displayed on the SLMs to generate the modes  $LG_{09}$  and  $LG_{0-9}$ . Figure 5(d) shows the captured intensity pattern, which again shows the “petal” beam shape, now with  $2\ell = 18$  azimuthal lobes distributed along a ring focusing with larger diameter compared to the results in Fig 3. Figure 5(c) shows the expected VB and Fig 5(d) shows the expected intensity distribution after the beam is filtered with a linear polarizer oriented at  $45^\circ$ .

Following the discussion in the previous subsection, these lobes are produced every  $20^\circ$ . Therefore, adding phase bias of  $\pi/8$  radians results in rotation of the petal pattern of  $20^\circ \times \left(\frac{\pi/8}{2\pi}\right) = 1.25^\circ$ . The experimental interferograms in Fig 6 illustrate this rotation. As expected, we observe the rotation of the pattern, but we require 3 steps to achieve the same rotation angles as in Fig 4. These images are used to calculate the phase difference distribution  $\alpha(x, y)$  of the superposition with the PSI synchronous detection in Eq (8). The result is presented in Fig 5(g) which now shows the expected 18 phase jumps, as simulated in Fig 5(f).

A completely different situation is obtained when the same hologram is displayed on LCoS1 and LCoS2 SLMs, thus encoding the same mode in both polarizations, in this case, the mode  $LG_{09}$ . The corresponding results are presented in Figs 7 and Fig 8. Note that in Figs 7(a) and 7(b), now we are addressing the same hologram in both SLMs. Now the generated beam is not a VB in the sense that the state of polarization is the same at all points, always linearly polarized (Fig 7(c)). The captured image in the CCD camera now presents a continuous ring of the same diameter as that in Fig 5(c), but now there is no azimuthal interference.

Now, when we apply phase bias steps of  $\pi/8$  radians we do not observe a rotation of the pattern, as the images in Fig 8 are showing. Instead, the total intensity oscillates in agreement with the calibration shown in Fig 2. These results demonstrate that we are generating a scalar vortex beam which has a uniform state of polarization. The phase bias only changes this state of polarization. Now, when the 16 images for this beam are used to calculate the phase difference distribution  $\alpha(x, y)$ , the result provides values of 0 (black) and  $2\pi$  (white) shown in Fig 7(g).

#### 5.4. Superposition of non-standard combinations of LG modes

To complete the results, we finish by presenting two additional cases where a non-standard combination of  $LG$  modes is encoded to generate arbitrary vector beams. In the next example, we apply the same technique to a vector beam generated by encoding  $LG$  modes with nonzero radial index. In this case we use the  $LG_{13}$  and  $LG_{1-3}$  modes. Like in previous cases, Fig 9(a) and 9(b) show the two phase-only holograms displayed on the LCoS1 and LCoS2 SLMs. Figure 9(c) shows the expected VB. Note how the two rings of light are generated, with a state of polarization that changes ellipticity azimuthally. The expected intensity pattern when projected to a polarizer oriented at  $45^\circ$  is shown in Fig 9(d), and the corresponding experimental captured intensity pattern in Fig 9(e). Now the pattern with six lobes is reproduced not only in the central annular ring (like in the case of  $LG_{03}$  and  $LG_{0-3}$  modes superposition in Fig 3), but a second ring appears also showing the same kind of interference.

The same kind of PSI experiment was conducted to derive the phase distribution. Like in the case shown in Fig 4, the addition of phase steps of  $\pi/8$  radian results in a rotation of the pattern in angular steps of  $3.75^\circ$ . The result of the PSI algorithm provides the phase pattern shown in Fig 9(g) which again shows 6 phase jumps in the angular coordinate, both in the inner circle and in the outer one, as expected from the simulation in Fig 9(f).

The final example that we include is the superposition of modes  $LG_{00}$  and  $LG_{07}$ . This kind of superposition, where the topological charge (azimuthal order) is different in each polarization, generates the so-called hybrid vector beams. Since one of the beams is the zero order Gaussian beam, this one will focus in a regular bright spot, while the  $LG_{00}$  mode will focus on a ring of light of relatively big diameter. Therefore,

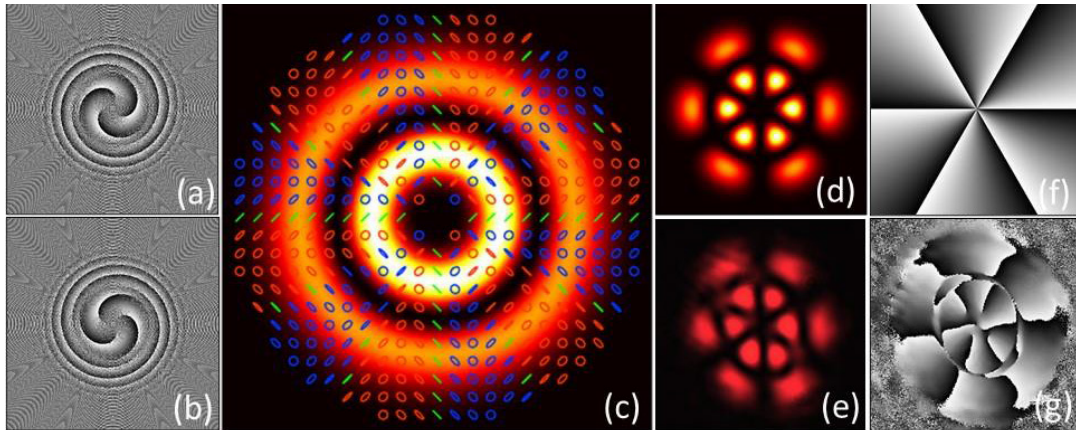


**Fig 9.** (a) and (b) Central part of the phase-only holograms displayed on LCoS1 and LCoS2 SLMs to generate  $LG_{13}$  and  $LG_{1,3}$  modes. (c) Simulation of the intensity and polarization of the generated vector beam. (d-e) Intensity distribution after passing through a polarizer oriented at  $45^\circ$ , simulation and experiment. (f) Phase difference  $\alpha(x, y)$ . (g) Result obtained by PSI synchronous algorithm.

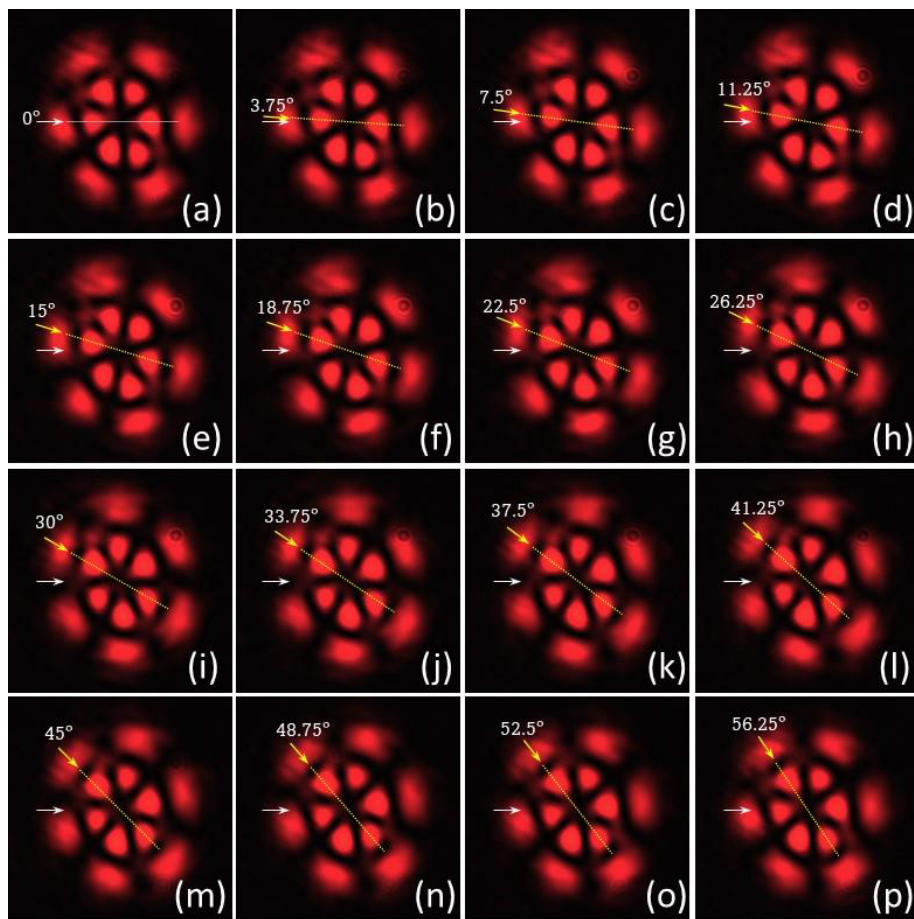


**Fig 10.** Sixteen interferograms with superposition of  $LG_{13}$  and  $LG_{1,3}$  using phase steps of  $\pi/8$ .

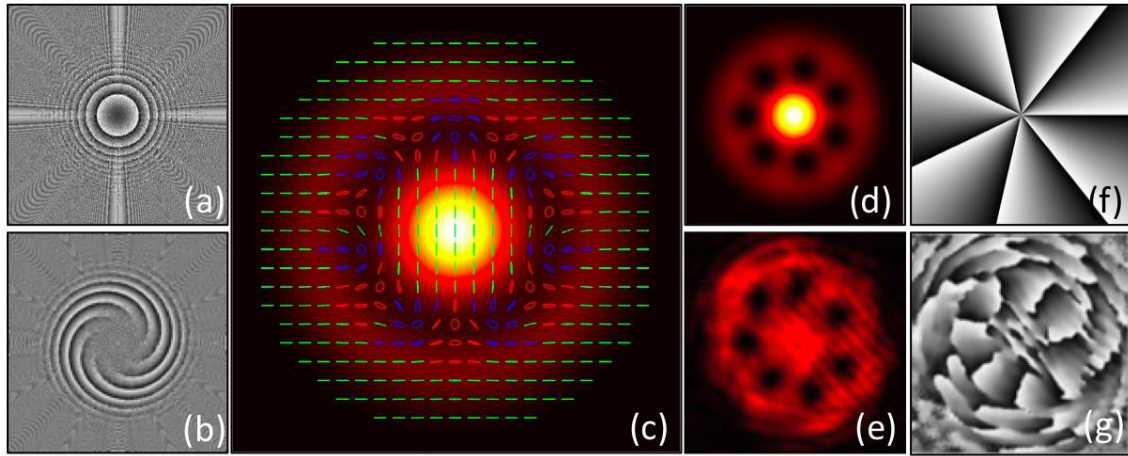


**Fig 11.** (a) and (b) Central part of the phase-only holograms displayed on LCoS1 and LCoS2 SLMs to generate  $LG_{00}$  and  $LG_{07}$  modes. (c) Simulation of the intensity and polarization of the generated vector beam. (d-e) Intensity distribution after passing through a polarizer oriented at  $45^\circ$ , simulation and experiment. (f) Phase difference  $\alpha(x, y)$ . (g) Result obtained by PSI synchronous algorithm.

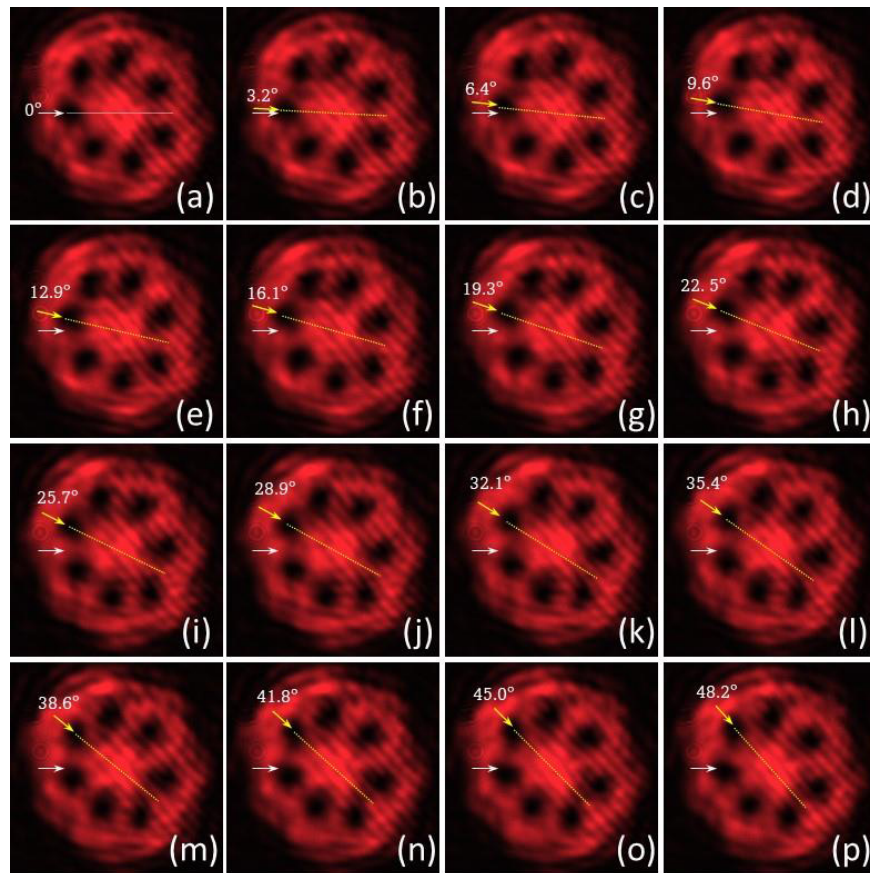


**Fig 12.** Sixteen interferograms with superposition of  $LG_{00}$  and  $LG_{07}$  using phase steps of  $\pi/8$ .

the interference is becoming more complicated since there is intensity variation along the radial direction and phase variation along the azimuthal direction. The expected VB is shown in Fig 11(c). Note how the central part of the beam, where the  $LG_{00}$  mode mainly focuses, is linearly polarized in the vertical direction. On the contrary, the outer part of the ring focus of the  $LG_{07}$  mode is also linearly polarized but horizontally. In between, in the region of superposition, the local state of polarization changes azimuthally. The intensity after passing through the polarizer at  $45^\circ$  (Fig 11(d)) and the corresponding experimental pattern shown in Fig 11(e), both show a beam with seven dark points all at the same distance from the centre.

These dark spots rotate as we add a phase bias in LCoS2 SLM, in angular steps of  $(360^\circ/7) \times (\frac{\pi/8}{2\pi}) = 3.21^\circ$ . Figure 12 shows all the experimental captures when adding the 16 phase steps of  $\pi/8$  radians. These images are again employed to calculate the phase difference distribution  $\alpha(x, y)$  shown in Fig 11(g) which, in the area of superposition of the two beams, shows the expected azimuthal variation.

## 6 Conclusions

In summary, we have presented new results for the generation of vector beams with a previously reported highly efficient optical system [27] that uses two LCoS-SLMs to encode two different Laguerre-Gauss modes onto two orthogonal states of polarizations (in all the provided examples, the linear horizontal-vertical states).

As a novelty, we demonstrate the capability of the same system to perform phase-shifting interferometry (PSI) to evaluate the phase function  $\alpha(x, y)$  given by the difference of the phases between the two encoded modes. PSI is achieved simply by adding a phase bias in one of the SLMs. Because the LCoS-SLMs provide continuous phase modulation, the number of steps for the PSI can be selected arbitrarily. In our case we selected 16 steps of  $\pi/8$  phase shift to provide a precise measurement through a synchronous detection algorithm.

## Acknowledgements

The authors acknowledge Dr José Luis Martínez-Fuentes and Dr David Marco Castillo for their help in optical experiments and computer simulations. This work has been financed by Ministerio de Ciencia, Innovación y Universidades, Spain (RTI2018-097107-B-C33).

## Note from the authors

Ignacio Moreno and María del Mar Sánchez-López conducted their studies of the Physics degree at Autonomous University of Barcelona (UAB), where they followed the course of Optics imparted by Prof. Yzuel. Later, Prof Yzuel was one of the supervisors of Moreno's Ph D Thesis. Pascuala García-Martínez has collaborated with Prof Yzuel in different activities in the frame of different scientific societies in the promotion of groups of Women in Physics and Women in Optics. We all feel privileged to have had the possibility to know Prof Yzuel and learn so much from her Physics, but also as a close teacher and a great person. Optics in Spain could not really be understood without the great efforts done by María Yzuel during all her career, and we feel very proud to be a direct witness of her unique trajectory and pioneering achievements.

## References

1. Dorn R, Quabis S, Leuchs G, Sharper focus for a radially polarized light beam, *Phys Rev Lett*, 91(2003)233901; doi.org/10.1103/PhysRevLett.91.233901.
2. Roxworthy B J, Toussaint K C(Jr), Optical trapping with  $\pi$ -phase cylindrical vector beams, *New J Phys*, 12 (2010) 073012; doi.org/10.1088/1367-2630/12/7/073012.

3. Jin Y, Allegre O J, Perrie W, Abrams K, Ouyang J, Fearon E, Edwardson S P, Dearden G, Dynamic modulation of spatially structured polarization fields for real-time control of ultrafast laser-material, *Opt Express*, 21(2013)25333–25343.
4. Török P, Munro P R T, The use of Gauss-Laguerre vector beams in STED microscopy, *Opt Express*, 12(2004) 3605–3617.
5. Forbes A, Laser Beam Propagation. Generation and Propagation of Customized Light, (CRC, Pretoria), 2014.
6. Rosales-Guzmán C, Ndagano B, Forbes A, A review of complex vector light fields and their applications, *J Opt*, 12, 123001 (2018); doi.org/10.1088/2040-8986/aaeb7d.
7. Mushiaki Y, Matsumura K, Nakajima N Y, Generation of radially polarized optical beam mode by laser oscillation, *Proc IEEE*, 60(1972)1107–1109.
8. Tidwell S C, Ford D H, Kimura W D, Generating radially polarized beams interferometrically, *Appl Opt*, 29 (1990)2234–2239.
9. Bomzon Z, Biener G, Kleiner V, Hasman E, Radially and azimuthally polarized beams generated by space-variant dielectric subwavelength gratings, *Opt Lett*, 27(2002)285–287.
10. Stalder M, Schadt M, Linearly polarized light with axial symmetry generated by liquid-crystal polarization converters, *Opt Lett*, 21(1996)1948-1950.
11. Marrucci L, Manzo C, Paparo D, Optical spin-to-orbital angular momentum conversion in inhomogeneous anisotropic media, *Phys Rev Lett*, 96(2006)163905; doi.org/10.1103/PhysRevLett.96.163905.
12. Cardano F, Karimi E, Slussarenko S, Marrucci L, de Lisio C, Santamato E, Polarization pattern of vector vortex beams generated by q-plates with different topological charges, *Appl Opt*, 51(2012)C1-C6.
13. Rafayelyan M, Brasselet E, Laguerre–Gaussian modal q-plates, *Opt Lett*, 42(2017)1966–1969.
14. Yao A M, Padgett M J, Orbital angular momentum: origins, behaviour and applications, *Adv Opt Photon*, 3(2011)161–204.
15. Gibson G, Courtial J, Padgett M J, Vasnetsov M, Pasko V, Barnett S M, Franke-Arnold S, Free-space information transfer using light beams carrying orbital angular momentum, *Opt Express*, 12(2004)5448–5456.
16. Milione G, Nguyen T A, Leach J, Nolan D A, Alfano R R, Using the non-separability of vector beams to encode information for optical communication, *Opt Lett*, 40(2015)4887–4890.
17. Trichili A, Rosales-Guzmán C, Dudley A, Ndagano B, Salem A B, Zghal M, Forbes A, Optical communication beyond orbital angular momentum, *Sci Rep*, 6(2016)27674; doi.org/10.1038/srep27674.
18. Vinu R V, Singh R K, Determining helicity and topological structure of coherent vortex beam from laser speckle, *Appl Phys Lett*, 109(2016)111108doi.org/10.1063/1.4962952.
19. Han Y, Zhao G, Measuring the topological charge of optical vortices with an axicon, *Opt Lett*, 36(2011)2017–2019.
20. Prabhakar S, Kumar A, Banerji J, Singh R P, Revealing the order of a vortex through its intensity record, *Opt Lett*, 36(2011)4398–4400.
21. Guo C.-S, Lu L.-L, Wang H.-T, Characterizing topological charge of optical vortices by using annular aperture, *Opt Lett*, 34(2009)3686–3688.
22. Dong M, Lu X Y, Zhao C, Cai Y, Yang Y, Measuring topological charge of partially coherent elegant Laguerre-Gaussian beam, *Opt Express*, 26(2018)33035–33043.
23. Schulze C, Dudley A, Flamm D, Duparré M, Forbes A, Measurement of the orbital angular momentum density of light by modal decomposition, *New J Phys*, 15, 073025 (2013); doi.org/10.1088/1367-2630/15/7/073025.
24. Moreno I, Davis J A, Badham K, Sánchez-López M M, Holland J E, Cottrell D M, Vector beam polarization state spectrum analyzer, *Sci Reports*, 7, 2216 (2017); doi.org/10.1038/s41598-017-02328-5.
25. Hu X, Gezhi Z, Sasaki O, Chen Z, Pu J, Topological charge measurement of vortex beams by phase-shifting digital hologram technology, *Appl Opt*, 57(2018)10300–10305.
26. Huang Y, Vinu R V, Chen Z, Sarkar T, Singh R K, Pu J, Recovery and characterization of orbital angular momentum modes with ghost diffraction holography, *Appl Sci*, 11, 12167 (2021); doi.org/10.3390/app112412167.
27. García-Martínez P, Marco D, Martínez-Fuentes J L, Sánchez-López M M, Moreno I, Efficient on-axis SLM engineering of optical vector modes, *Opt Lasers Eng*, 125, 105859 (2020); doi.org/10.1016/j.optlaseng.2019.105859.

28. Creath K, Phase-Shifting Holographic Interferometry, in *Holographic Interferometry - Principles and Methods*, (Ed) Rastogi P K, (Springer, Berlin, Heidelberg), 1994, pp 109–150.
29. Greivenkamp J E, Bruning J H, Phase Shifting Interferometry, in Malacara D (Ed): *Optical Shop Testing*, (Wiley, New York), 1992, pp 501–598.
30. Moreno I, Sánchez-López M M, Davis J A, Cottrell D M, Simple method to evaluate the pixel crosstalk caused by fringing field effect in liquid-crystal spatial light modulators, *J Eur Opt Soc, – Rapid Pub*, 17(2021)27; doi.org/10.1186/s41476-021-00174-7.
31. Martínez J L, García-Martínez P, Moreno I, Microscope system with on axis programmable Fourier transform filtering, *Opt Lasers Eng*, 89(2017)116–122.
32. Martínez-Fuentes J L, Moreno I, Random technique to encode complex valued holograms with on axis reconstruction onto phase-only displays, *Opt Express*, 26(2018)5875–5893.
33. Galvez E J, Vector beams in free space, Chap 3, in *The Angular Momentum of Light*, (Eds) Andrews D L, Babiker M, (Cambridge University Press), 2013.
34. de Groot P, Phase Shifting Interferometry, in *Optical Measurement of Surface Topography*, (Ed) Leach R, (Springer, Berlin, Heidelberg), 2011.
35. Phase Estimation in Optical Interferometry, (Eds) Rastogi P, Hack E, (CRC Press), 2015.
36. Messaadi A, Sánchez-López M M, García-Martínez P, Vargas A, Moreno I, Optical system for measuring the spectral retardance function in an extended range, *J Eur Opt Soc – Rapid Pub*, 12, 21 (2016); doi.org/10.1186/s41476-016-0023-7.
37. Litvin I A, Burger L, Forbes A, Petal-like modes in Porro prism resonators, *Opt Express*, 15(2007)14065–14067.

[Received: 19.01.2022; accepted; 01.04.2022]



Pascuala García-Martínez is Full Professor of Optics at the Optics Department in the University of Valencia. She received her BS degree in physics in 1993 from the University of Valencia, Spain. She received her MS and Ph D degrees from the same university in 1995 and 1998, respectively. She was an invited researcher in Georgia Tech Lorraine, Metz (France), Faculty of Electrical Engineering, Tel-Aviv University (Israel) and Centre d'Optique, Photonique et Lasers, Université Laval, Québec (Canada). She has also visited as researcher different spanish universities as the University of Alicante and the University Miguel Hernández of Elche where currently she is developing her research as member of the group (Grupo de Tecnologías Ópticas y Optoelectrónicas). Prof Garcia-Martinez's major research interests include optical image processing and spatial light modulators, specifically liquid crystals applied to diffraction and polarization. She has been invited by European Erasmus program to teach in Ecole Nationale Supérieure de Physique de Marseille, Université d'Aix Provence, in Marsella (France).

She has received the honorable mention of being Fellow member of SPIE (International Society for optics and photonics) in 2021 and Senior of the OSA (Optical Society of America) in 2015. She has been part of several SPIE organization and management committees.

Deeply committed to defending women's rights researchers: She is the president of the Women in Physics specialized group of the Real Sociedad Española de Física (RSEF). She also is an active defender of gender actions in science teaching seminars and courses. She is member of the board of directors of AMIT (Asociación de Mujeres Investigadoras y Tecnólogas). Currently is member of the Comission for Equality Policies of the University of Valencia, and she presides the gender equality commission of the Faculty of Physics.



Ignacio Moreno is Full Professor of Optics at University Miguel Hernández (UMH), in Elche, Spain. He received the degree in Physics and the Ph D in Physics in 1992 and 1996, respectively at the Autonomous University of Barcelona. His Ph D thesis focused on the application of spatial light modulators to the realization of a programmable optical correlator system, supervised by Prof María J Yzuel and Prof. Juan Campos. For two years (1996-98) he joined the Department of Optics of the University of Valencia, and since 1998 he is at the Department of Materials Science, Optics & Electronics Technology at UMH. In 2020 he joined the UMH Institute of Bioengineering.

He has an extensive research experience in the field of liquid crystal spatial light modulators, and their applications in diffractive and polarization optics, having published more than 150 articles in peer reviewed journals. He maintains stable active collaborations with Spanish (Autonomous University of Barcelona, University of Valencia) and international centers (San Diego State University (USA), Institut FEMTO, Université de Franche-Comté (France) and Universidad de La Frontera (Chile)). He is Senior Member and Fellow Member of SPIE – The International Society for Optics and Photonics (2009 and 2014, respectively), and Senior Member and Fellow Member of Optica – The Optical Society (2010 and 2017, respectively). In 2012 he received the EOS2012 Prize from the EOS – European Optical Society. In 2015 he became a grantee of the Fulbright Scholar Program.

In 2017-20 was President of the Spanish Society of Optics – SEDOPTICA. Previously, in 2014-2017, he was Vice President of SEDOPTICA; and in the period 2005-2014 he was editor of the journal *Óptica Pura y Aplicada* – OPA. Since 2013 he is Associate Editor of the journal "Optical Engineering". He has been Guest Editor of two special sections entitled "Liquid Crystals for Photonics (2011), and on Spatial Light Modulators: Devices & Applications (2019)". In 2015, he was member of the Spanish Committee for the International Year of Light, and since 2017 he is Vice President of the Spanish Committee for the International Day of Light. He was the President of the Organizing Committee of two meetings held at Elche: the 4th Spanish Meeting on Optoelectronics – Optoe'05 (July 2005) and the 3rd International Workshop on Liquid Crystals for Photonics (September 2010). In the period 2007-2016 he was Director of TECNIT Doctoral Program, the UMH PhD Program in Industrial and Telecommunication Engineering.



María del Mar Sánchez-López is Full Professor of Applied Physics at Universidad Miguel Hernández (UMH), in Elche, Spain. She graduated in Physics in 1992 and got her Ph D in Physics in 1997, both at Universitat Autònoma de Barcelona. After her Ph D Thesis on the electronic structure of high-Tc superconductors, and a post-doc grant (1997-98) of INFN, Istituto Nazionale per la Fisica Della Materia, Italy), she joined the Electronics Technology area in UMH, and since 2005 she is with the Applied Physics Department.

After joining UMH her research activities geared toward Photonics. She was an invited researcher in the electro-optics laboratory at San Diego State University (California) in 2002, 2015 and 2017, and at the Laboratoire d'Optique P. M. Duffieux in Institut FEMTO ST of Besançon (France) in 2006. Her research activity is actually centered on vector light beams, slow and fast-light, and liquid-crystal based reconfigurable systems for spectral shaping. Her research experience has led to about 70 papers in JCR journals, and has participated in 25 competitive research projects. Dr. Sánchez-López is also active in outreach activities in photonics and in promoting women in STEM.

She helped organizing, as part of the local Committee, the 4th Reunión Española de Optoelectrónica (OPTOEL, July 2005) and the 3rd International Workshop on Liquid Crystals for Photonics (September 2010). In 2015 she was recognized as Senior Member of SPIE-The International Society for Optics and Photonics (<http://spie.org/x19144.xml>), and has participated in the 2014-2015 SPIE Women in Optics Planner and in the 2017 SPIE Gender Equity Survey. She is also a member of SEDOPTICA – Sociedad Española de Óptica and RSEF – Real Sociedad Española de Física, where she became President of its Local Section of Alicante in February 2017 until June 2021. She is now the photonics representative of the academic committee in TECNIT Doctoral Program, the UMH Ph D Program in Industrial and Telecommunication Engineering.